Shear flow and drift wave turbulence dynamics in a cylindrical plasma device

Z. Yan,[1,2] G. R. Tynan,[1] C. Holland,[1] M. Xu,[1] S. H. Müller,[1] and J. H. Yu[1]
[1]*Center for Energy Research, University of California–San Diego, California 92093, USA*
[2]*Department of Engineering Physics, University of Wisconsin–Madison, Wisconsin 53706, USA*

(Received 10 August 2009; accepted 19 January 2010; published online 8 March 2010)

The experimental observations of the dynamics of the coupled drift wave turbulence (DWT)/sheared zonal flow (ZF) system in a cylindrical plasma device using a combination of Langmuir probe and fast-framing imaging measurements are reported. The results show the presence of an azimuthal ZF that exhibits low frequency (~250 Hz) fluctuations. The envelope of the higher frequency (above 5 kHz) floating potential fluctuations associated with the DWT, the density gradient, and the turbulent radial particle flux are all modulated out of phase with the strength of the ZF. The divergence of the turbulent Reynolds stress is also modulated at the same slow time scale in a phase-coherent manner consistent with a turbulent-driven shear flow sustained against the collisional and viscous damping. The radial turbulence correlation length and cross-field particle transport are reduced during periods of strong flow shear. The results are qualitatively consistent with theoretical expectations for coupled DWT-ZF dynamics. © *2010 American Institute of Physics*. [doi:10.1063/1.3322823]

I. INTRODUCTION

Heat and particle transport in magnetically confined fusion plasmas is due to turbulent transport driven by pressure gradient-driven instabilities. One of the key issues of the fusion research is to understand the underlying physics of this turbulent transport, which results in particle and heat fluxes that are significantly larger than that which results from "classical and neoclassical transport theory."[1] The relationship between the fluxes and the mean gradients is of particular interest since this is what determines to a large degree the system size needed for a positive energy gain. Theory and simulation have both suggested that the saturation of drift wave turbulence (DWT) occurs via the generation of linearly damped radially sheared poloidally and toroidally extended plasma flows denoted as zonal flows (ZFs) via the action of the DWT Reynolds stress,[2,3] which acts to nonlinearly transfer turbulence energy into a large-scale damped motion that does not yield transport itself.

The ZFs have been viewed theoretically as being generated by a nonlinear modulation instability in which a small seed shear flow acts to scatter DWT energy into the shear flow itself, resulting in an amplification of the original seed shear and producing a turbulent-driven sheared flow that is denoted as the ZF. The amplification of the ZF comes at the expense of the DWT energy. Thus as the ZF grows, the DWT energy should decrease in this picture. Theoretically the total energy of the coupled DWT-ZF system is conserved in this interaction, and the DWT radial wavenumber is increased due to the random shearing effect of the ZF. If most of the energy goes into the ZF, resulting in smaller DWT energy, eventually eliminating the nonlinear drive of the ZF. As a result the ZF decays away (usually via a process that is assumed to be linear). The background plasma pressure gradient, which is sustained by a constant external heat input, then leads to the growth of DWT energy, and the cycle is then repeated. If cross-field transport is interrupted for a significant period of time, the plasma pressure profile can then respond, resulting in a change to the underlying drive of the DWT. Detailed reviews of the theoretical elements of this picture are available in the literature;[3,4] a summary of the experimental status of the subject is also available.[5]

A complete experimental demonstration of the theoretical picture of the above DWT-ZF dynamics requires several simultaneous observations to be made in the same experimental apparatus. First, the existence of a radially sheared azimuthal flow must be demonstrated. Second, the shear flow should be sustained by the turbulent Reynolds stress against collisional and viscous damping in order to distinguish it from so-called mean shear flows, which are, by definition, sustained by nonturbulence processes such as the return current associated with ion orbit losses in toroidal devices[6] or the ion pressure gradient associated with transport barrier formation.[7] This can be done in configuration space by looking at the turbulent momentum conservation equation[8] or in the Fourier domain using bispectral techniques.[7,9] Third, the ZF shear should be strong enough to reduce the radial correlation length of the turbulent fluctuations, which is a key element in the shear flow dynamics. Finally, the ZF kinetic energy should increase at the expense of the turbulent kinetic energy, while the total kinetic energy is conserved. Qualitatively this could be manifested by an anticorrelation between the high frequency turbulence kinetic energy and the low frequency kinetic energy. Observations of some of these predictions have been reported in the literature, but to our knowledge no complete set of such measurements from a single experiment exists. In this paper we show that all of these theoretically predicted behaviors indeed occur simultaneously in a simple plasma system that is amenable to the detailed multifield, multipoint turbulence measurements

necessary to examine the fundamental physics of the coupled DWT-ZF system.

The rest of the paper is organized as follows. In Sec. II we briefly describe our experimental setup. In Sec. III, we show that the shear flow varies slowly in time and that this slow variation is associated with slow variations in the turbulence statistics. In Sec. IV we examine the back-reaction of the shear flow on the turbulence and show via direct imaging the essential elements of the shear decorrelation process. In Sec. V we discuss the experimental results, and lastly in Sec. VI we summarize our results.

II. EXPERIMENTAL SETUP

The experiments described here are carried on the Controlled Shear Decorrelation eXperiment (CSDX), a linear cylindrical laboratory plasma device powered with an $m=0$ azimuthally symmetric helicon antenna. The machine is a stainless steel cylindrical vacuum chamber with overall length 2.8 m and a diameter of 20 cm surrounded by a set of electromagnet coils that can generate a uniform up to 0.1 T magnetic field. Plasma is generated by a 13.56 MHz, 1500 W rf helicon wave source equipped with a matching circuit that is adjusted such that less than 30 W of power is reflected. The typical working gas pressure is $P=3$ mTorr in argon. The typical peak plasma density is $\sim 10^{19}$ m^{-3}, electron temperature is ~ 3 eV, the ion temperature is $\sim 0.5-0.7$ eV, and the neutral gas temperature is ≤ 0.4 eV based on measurements of ion and neutral argon Doppler broadening for 1500 W/0.1 T/3 mTorr, the operating conditions used in these experiments. The plasma source radius is $\sim 4.5-5.0$ cm, resulting in a steep electron pressure gradient located at $r \sim 3$ cm. The magnetic field lines exiting the two ends of the device terminate on insulating surfaces to eliminate the possibility of currents flowing through the end plates of the device. Thus the axial current associated with the drift waves must be balanced by cross-field currents carried by ion polarization drifts (which are equivalent to the turbulent Reynolds stress[10]). A more detailed description of the machine can be found in Refs. 11 and 12.

The measurements of the fluctuating plasma density, potential, and the electric fields along with the resulting turbulent Reynolds stress are made by a multitip Langmuir probe.[13] The probe tips are arranged as two 3×3 array, which are shifted by 1.5 mm along the magnetic field. The radial displacement of the probe tips is 1.5 mm, and the azimuthal displacement is 2.5 mm. A schematic of the probe can be found in Ref. 13. This probe tip arrangement allows the calculation of the radial and the azimuthal electric field, as well as the radial gradient of the fluctuation quantities at the same radial location. A digitizer sampling at 500 kHz is used to record the data. The resulting Nyquist frequency is 250 kHz, well above all fluctuation frequencies. Samples are obtained for a duration of 2 s at each radial location, allowing for low-variance estimation of the fluctuation statistics.

Two mirrors are placed at the end of the machine to reflect the visible light emission from plasma to a Celestron C11-SGT(XLT) telescope located approximately 8 m away from the focal plane located within the plasma column. A Phantom v.7 fast-frame camera is used to capture the plasma motion through the telescope. Since the telescope has a very small angular field of view ($\sim 0.71°$), the angular field of view of the camera is close to parallel to the magnetic fields, thus virtually eliminating parallax effects that can mask parallel dynamics as radial motion. The frame rate is 97 560/s for the 128×64 resolution, and a Pentax 25 mm f/1.4 lens is used to couple the light from the telescope to the camera in these experiments. When capturing these images, the camera is focused on the axial location where probe is inserted radially (although usually the probe is not inserted during such imaging measurements). A more detailed discussion of this imaging diagnostic is being prepared for publication elsewhere.

III. EVIDENCES OF THE SLOW EVOLVING SHEAR FLOW

Previous work has demonstrated the onset of collisional drift waves in the device and has documented their transition to a state of weak DWT.[12] In addition, the existence of a time-averaged radially sheared azimuthally symmetric plasma fluid flow at the interface region located between 3.5–4 cm has been shown to be consistent with the experimentally observed turbulent Reynolds stress for reasonable estimates of the collisional ion-ion viscosity and ion-neutral drag[8,13,14]—signatures that are consistent with the interpretation of this flow as a ZF. In these earlier works, the shear flow dynamics were averaged over multiple statistical ensembles, resulting in a time-averaged view of the shear flow and of the turbulence statistics. In this paper we investigate the temporal dynamics of the ZF-DWT system.

The Phantom v.7 fast-frame camera is used to capture the visible light emission from the plasma through the telescope. No interference filter is used and thus the measurements integrate over the entire visible spectrum. However, most of the light emission occurs from a combination of neutral Ar–I (750 nm) and singly ionized Argon (488 nm) emission. In this work, a total of 24 000 (~ 240 ms) frames images are recorded and used in the analysis. The light intensity of the image is somewhat correlated with the plasma density,[15] but it is also likely to be influenced by the electron temperature and the neutral density. The detailed relationship between these plasma discharge quantities and the light intensity is currently under investigation and will be discussed in a future publication. Regardless of this fact, we can still gain insight into the turbulence dynamics from the fast-framing imaging.

The azimuthal symmetry of the ZF is best shown by examining images obtained with the fast-framing camera observing the visible light intensity fluctuations associated with the DWT fluctuations.[15] To obtain the intensity fluctuation images, we first perform a time average image from 2000 frames and then subtract this mean image from each frame. Applying the two-dimensional (2D) time-delay estimation (TDE) technique to a time-sequence of these images, we obtain the 2D time-averaged flowfield in the plane normal to the magnetic field. Here the 2D TDE is an extension of the 1D TDE technique,[16] i.e., instead of computing cross-

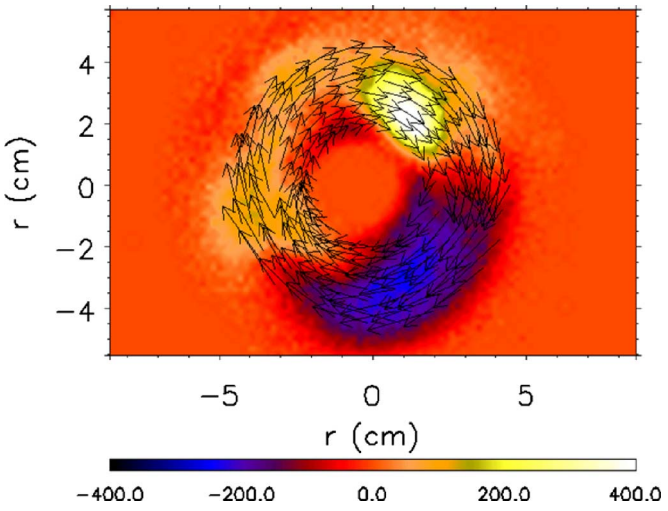

FIG. 1. (Color online) 2D flowfield obtained from 2D TDE technique on the fast-framing imaging.

correlation between two azimuthally separated data sets, compute the cross-correlations between a reference point located at (x_0,y_0) and points located in a square range from (x_0-L,y_0-L) to (x_0+L,y_0+L) with a series given time lag τ increasing from $\tau=0$ with a time step $\Delta\tau$. At each time lag τ the location of the maximal cross-correlations (x_τ,y_τ) is found, and the velocity is computed from $v_x=(x_\tau-x_0)/\tau$ and $v_y=(y_\tau-y_0)/\tau$. Then the velocity at point (x_0,y_0) is an average of all the velocities at different τ. Here we choose L to be 16 pixels, corresponding to about 2.4 cm, and $\Delta\tau$ to be 6 μs (imaging data were interpolated by a factor of 10). In computing each cross-correlation, we use ~1 ms time window and then ensemble average all the windows to get an averaged cross-correlation function. The 2D flowfield is shown in Fig. 1 by arrows overlay on the intensity fluctuations (color bar is an arbitrary unit). At $r\sim3.6$ cm the rms deviation of the azimuthal velocities $v_\theta(\theta)$ is only 11% of the azimuthally averaged $v_\theta(\theta)$, showing that the $m=0$ component to the azimuthal flow indeed exists as is a dominant component of the azimuthal flow. A previous study has shown that this measured velocity is composed of a smaller electron diamagnetic drift component and a larger fluid flow associated with an $m=0$, $E\times B$ flow, which is also in electron drift direction.[16] Thus we take the motion of the fluctuations to represent to lowest order the motion of the plasma fluid.

The radial profile of the time-varying azimuthal shear flow is found by azimuthally averaging the TDE flowfield at each radial location for each available time (~1 ms of each time window, but no ensemble average is used in computing the cross-correlation). Several radial profiles at different times are shown in Fig. 2(a). The azimuthal flow is found to gradually develop a sheared profile, which then decays back to a flow profile that is close to solid body rotation and then the process repeats. Figure 2(b) shows the time history of the $V_\theta(t)$ obtained at $r=3.6$ cm, illustrating this time variation. A probability distribution function (PDF), computed as the histogram of the $V_\theta(t)$ at $r=3.6$ cm normalized by the time-averaged $V_\theta(t)$, is shown in Fig. 3. This PDF shows that the most probable velocity is approximately 80% of the time-

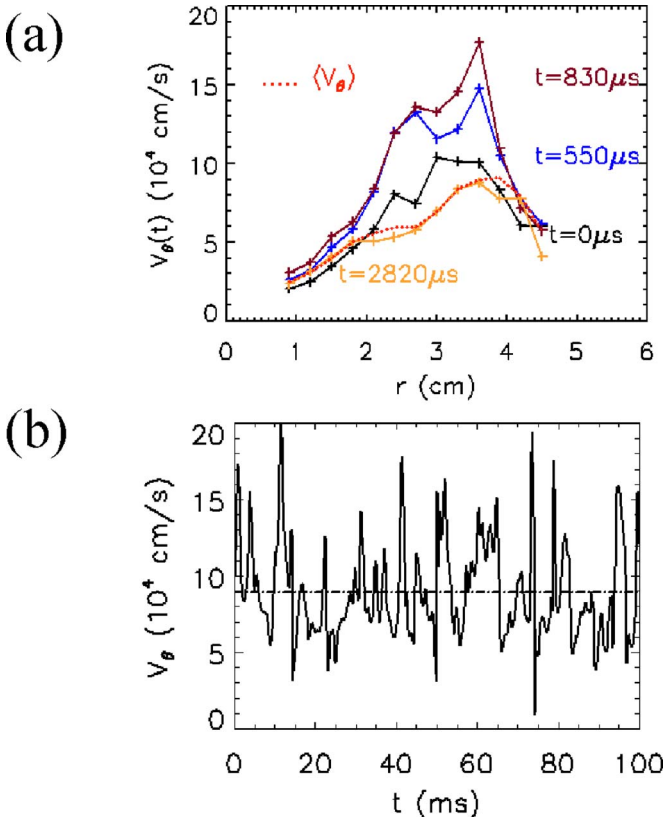

FIG. 2. (Color online) (a) Radial profiles of azimuthal flow obtained from azimuthally averaging the visible light TDE flowfield for different observation times. A radially sheared flow is observed to grow and decay with a period of ~4 ms. (b) Time-varying azimuthal flowfield at $r\sim3.6$ cm.

averaged $V_\theta(t)$ and the distribution is non-Gaussian and asymmetric over that time average. This suggests that the time-evolving shear flow behaves like a bursty event, spending more time in a condition of weaker shear flow [see Fig. 2(a), yellowish line at around 2820 μs, for example] than in a condition of stronger shear flow [see Fig. 2(a), red line at around 830 μs, for example). The frequency spectrum of V_θ shows that the mean frequency of this oscillation is around

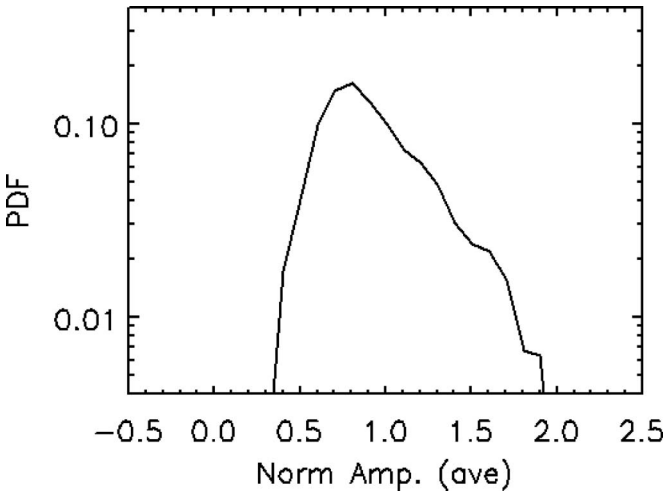

FIG. 3. PDF of the $v_\theta(t)$ at $r\sim3.6$ cm [normalized by the time-averaged $v_\theta(t)$] (log 10).

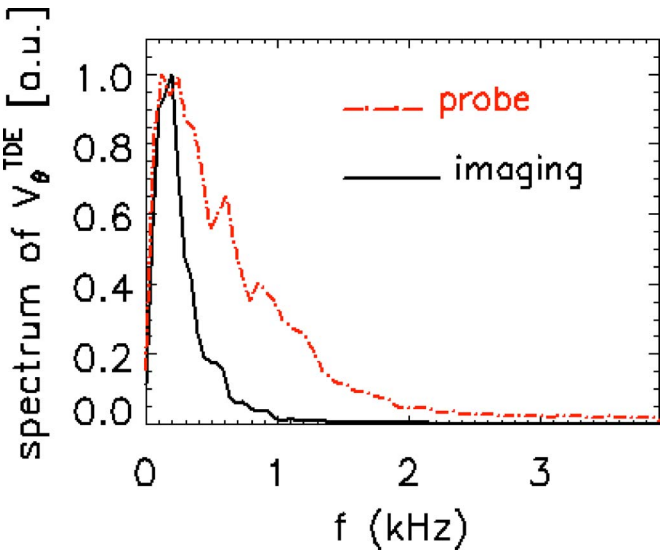

FIG. 4. (Color online) Spectrum of the time-varying azimuthal velocity field at the shear location (r=3.6 cm) from visible light velocimetry (solid line) and from Langmuir probe measurements (dot-dashed solid line).

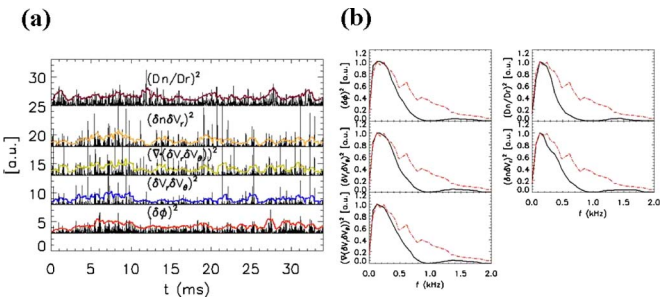

FIG. 5. (Color online) (a) Square of the turbulent floating potential, turbulent Reynolds stress, divergence of the turbulent Reynolds stress, and turbulent radial particle flux and their envelopes. (b) Spectra of the envelopes of the turbulent floating potential, turbulent Reynolds stress, divergence of the turbulent Reynolds stress, and turbulent radial particle flux. The dot-dashed line on each figure is the spectrum of the azimuthal velocity field.

250 Hz (Fig. 4, black solid line); the oscillation is clearly not coherent as the width of the frequency spectrum is also several hundred hertz. Our previous studies of the shear flow in CSDX and the relationship to the turbulent Reynolds stress[8,14] used large numbers of statistically independent ensembles, and thus those prior results represent a time-averaged view of this slowly oscillating shear flow and are close to (less than 20% difference) the time-averaged flow-field obtained in this experiment from fast-framing imaging, as shown by the red dots in Fig. 2(a).

The earlier results showed that the time-averaged shear flow was consistent with the time-averaged Reynolds stress and estimated flow damping profiles. Thus the question arises: how does the slow variation in the shear flow affect the turbulence? In order to address this question, the time-varying azimuthal velocity field is also measured with two azimuthally separated probe tips (separation distance of 5 mm) measuring floating potential by using TDE technique[16] with a serial of overlapping time windows that are each 1 ms long. The frequency spectrum of the time-varying shear flow measured with the probe is shown in Fig. 4 as the red dot-dashed line. Again, the shear flow is found to vary with a low frequency of about 250 Hz and has a frequency width also in the order of 100 Hz, consistent with the results obtained with the fast imaging. The differences in the higher frequency range may because that the azimuthal velocity from imaging is constructed from an azimuthally averaged 2D velocity as explained above, and as a result, this averaging process naturally washes out structures whose azimuthal extent is less than the circumference (i.e., structures with $m>0$). Since the frequency is associated with the azimuthal scale length, the higher frequency events are thus averaged out. The probe-based measurements do not azimuthally average the data, and thus the spectra of the probe measurements retain higher frequency information.

To investigate if the turbulence is also modulated at the same frequency, we look at the envelopes of the fluctuation quantities, such as fluctuation floating potential, turbulent Reynolds stress, divergence of the turbulent Reynolds stress, the turbulent radial particle flux, and density gradient, obtained by applying a high pass filter (using a 5 kHz cutoff frequency) to each instantaneous fluctuating quantity measured by the multitip probe array and then taking the square of the filtered result. The envelopes are found by applying a smoothing function with a ~1 ms time window to the filtered fluctuations. Figure 5(a) shows the square of the fluctuating floating potential, turbulent Reynolds stress, divergence of the turbulent Reynolds stress, the turbulent radial particle flux, and density gradient, as well as their envelopes, which are shown as the colored line on each panel. A spectral analysis of these envelopes demonstrates that they are all modulated with the same frequency as the shear flow evolution [Fig. 5(b)]. The red dot-dashed line on the panels in Fig. 5(b) shows the spectrum of the azimuthal velocity field from probe measurement. Clearly the fluctuating envelopes exhibit low frequency temporal evolutions that are nearly identical to that of the slowly varying sheared flow. To further look at the modulation effect of the shear flow, we compute the cross-correlation between envelops of the density gradient, floating potential fluctuations, particle flux, and the flow velocity at shear layer (~3.6 cm), respectively, for 2 s duration data, as shown in Fig. 6. It is found that there are finite anticorrelations. The values are lower than expected but are above the statistical significant value. It shows that the high frequency fluctuations are modulated out of phase with the ZF.

Keeping in mind our previous results linking the time-averaged shear flow and the time-averaged Reynolds stress, these results suggest that the variation in fluctuations may cause a slowly varying Reynolds stress, which can in turn be linked with the slowly varying sheared flow. Therefore, to test this possibility and investigate the modulation of the turbulent Reynolds stress with ZF, we must carefully consider the turbulent momentum balance equation.

For the collisional plasmas found in these experiments, the azimuthal component of the ion momentum equation is[14]

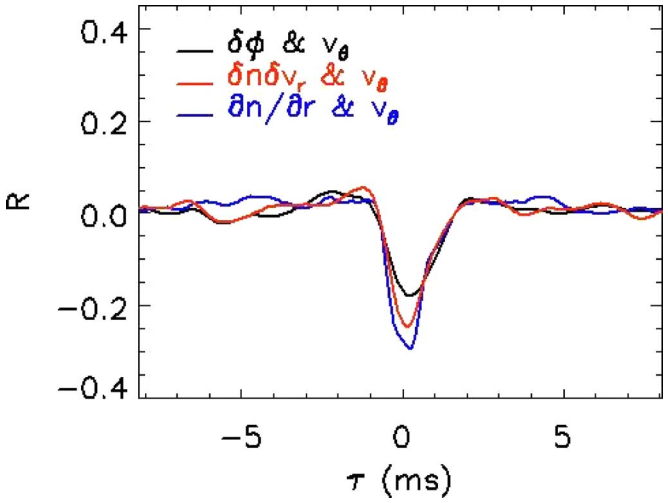

FIG. 6. (Color online) Cross-correlation between envelopes of floating potential, density gradient, particle flux, and flow velocity at shear layer.

$$\frac{\partial V_\theta}{\partial t} + V_r\frac{\partial V_\theta}{\partial r} + \frac{V_\theta}{r}\frac{\partial V_\theta}{\partial \theta} + V_z\frac{\partial V_\theta}{\partial z} + \frac{V_r V_\theta}{r} = \frac{e}{m}(E_\theta - V_r B) - \upsilon_{i-n}V_\theta + \mu_{ii}\left(\nabla^2 V_\theta + \frac{2}{r^2}\frac{\partial V_r}{\partial \theta} - \frac{V_\theta}{r^2}\right), \tag{1}$$

where υ_{i-n} is ion neutral collision rate and μ_{ii} is the ion viscosity and where we assume neutrals have negligible velocity, ion pressure fluctuation is negligible since the ion temperature is low (~0.5 eV) and an incompressible velocity fluctuations. Our observations show that the plasma rotates once azimuthally in about 0.5 ms, while the azimuthal velocity oscillation time scale is approximately 4 ms. We therefore chose an intermediate time scale of 1 ms over which we average this equation. This choice will average over the mode number $m>0$ turbulence but will still (roughly) resolve the slowly varying sheared azimuthal flow that has been shown to exist in the above results. Introducing the fluctuating radial and azimuthal velocities $\tilde{V}_r$ and $\tilde{V}_\theta$ and denoting the azimuthal flow that survives the 1 ms time averaging operation as $\langle V_\theta\rangle_t$, the turbulent momentum conservation equation can then be reduced to

$$\frac{\partial\langle V_\theta\rangle_t}{\partial t} + \frac{1}{r^2}\frac{\partial}{\partial r}(r^2\langle\tilde{V}_r\tilde{V}_\theta\rangle_t) = -\upsilon_{i-n}\langle V_\theta\rangle_t + \mu_{ii}\left(\frac{\partial^2\langle V_\theta\rangle_t}{\partial r^2} + \frac{1}{r}\frac{\partial\langle V_\theta\rangle_t}{\partial r} - \frac{\langle V_\theta\rangle_t}{r^2}\right), \tag{2}$$

where $\langle\ \rangle_t$ denotes 1 ms time window average. A detailed derivation can be found in Ref. 14. For simplicity and since no other measurements are available, the dissipation coefficients are assumed to be time stationary and to have values similar to those reported earlier.[8] From the multitip Langmuir probe the slow (1 ms) variation in the turbulent Reynolds stress and the azimuthal velocity field from TDE technique at shear location (~3.6 cm) are calculated. Both quantities are averaged over 1 ms time window, allowing a comparison of the inertial term

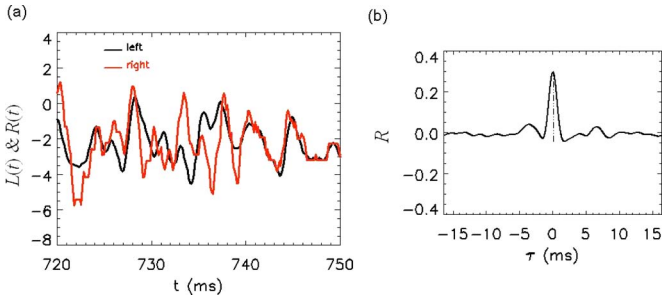

FIG. 7. (Color online) (a) Time traces of the left hand side and the right hand side of the ion momentum equation. (b) Cross-correlation between the left and the right hand sides of the momentum equation.

$$L(t) = \frac{\partial\langle V_\theta^{\mathrm{TDE}}\rangle_t^{\mathrm{probe}}}{\partial t} + \frac{1}{r^2}\frac{\partial}{\partial r}(r^2\langle\tilde{V}_r\tilde{V}_\theta\rangle_t^{\mathrm{probe}}), \tag{3}$$

and the force due to dissipation,

$$R(t) = -\upsilon_{i-n}\langle V_\theta^{\mathrm{TDE}}\rangle_t^{\mathrm{probe}} + \mu_{ii}\left(\frac{\partial^2\langle V_\theta^{\mathrm{TDE}}\rangle_t^{\mathrm{probe}}}{\partial r^2} + \frac{1}{r}\frac{\partial\langle V_\theta^{\mathrm{TDE}}\rangle_t^{\mathrm{probe}}}{\partial r} - \frac{\langle V_\theta^{\mathrm{TDE}}\rangle_t^{\mathrm{probe}}}{r^2}\right). \tag{4}$$

Figure 7(a) shows the time traces of $L(t)$ and $R(t)$ obtained in this manner. There are clearly some instances when the two sides of the momentum balance have a similar time variation, while at other times there appears to be little relationship between the two time series. The cross-correlation between $L(t)$ and $R(t)$ allows the statistical relationship to be better quantified. The result [Fig. 7(b)], which is computed independently from probe measured Reynolds stress and the azimuthal velocity fields, has a finite in-phase correlation of around 0.3–0.4, a value that is well above the statistical significant level of ~0.05. Although this peak value is lower than expected (probably due to the combined errors arising from the use of floating potential in place of plasma potential, the error associated with the finite differencing of the spatial gradients, the poor scale separation of the different temporal scales, and the assumption that the dissipation rates are fixed), the result does show that there is clear in-phase variation between the slow evolving shear flow and slowly evolving turbulent Reynolds stress against the collisional and viscous damping, qualitatively consistent with our earlier published results showing that the time-averaged shear flow is maintained against flow damping by the turbulent Reynolds stress.

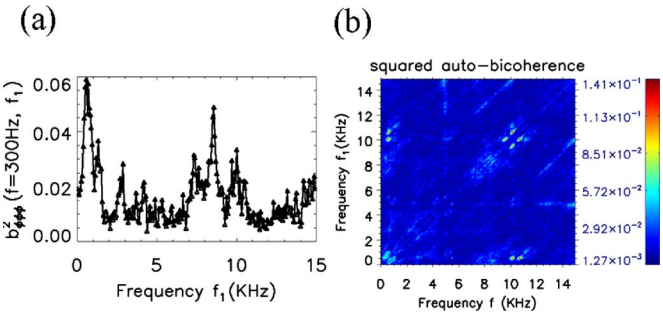

FIG. 8. (Color online) (a) Autobicoherence of the floating potential fluctuations $b^2(f=300\ \text{Hz}, f_1)$ for $f=f_1+f_2=300$ Hz at $r\sim3.6$ cm. (b) 2D autobicoherence of the floating potential fluctuations $b^2(f,f_1)$ at $r\sim3.6$ cm.

We further illustrate the relationship between the slowly varying shear flow and the turbulence statistics by examining the autobicoherence of floating potential fluctuation, which provides a measure of the phase coherence between fluctuations at two frequencies f_1 and f and which is defined as[17]

$$\hat{b}^2_{XXX}(f,f_1) \equiv \frac{|\hat{S}_{XXX}(f_1,f_2)|^2}{\frac{1}{M}\sum_{k=1}^{M}|X^{(k)}(f)|^2\frac{1}{M}\sum_{k=1}^{M}|X^{(k)}(f_1)X^{(k)}(f_2)|^2} = \frac{\left|\frac{1}{M}\sum_{k=1}^{M}X^{(k)}(f)X^{*(k)}(f_1)X^{*(k)}(f_2)\right|^2}{\frac{1}{M}\sum_{k=1}^{M}|X^{(k)}(f)|^2\frac{1}{M}\sum_{k=1}^{M}|X^{(k)}(f_1)X^{(k)}(f_2)|^2}, \tag{5}$$

where $\hat{S}_{XXX}(f_1,f_2)$ is the bispectrum of floating potential fluctuations defined as

$$\hat{S}_{XXX}(f_1,f_2) \equiv E[X(f)X^*(f_1)X^*(f_2)] = \frac{1}{M}\sum_{k=1}^{M}X^{(k)}(f)X^{*(k)}(f_1)X^{*(k)}(f_2). \tag{6}$$

In the above equations (k) indicates the kth realization, M is the total number of realizations, and the symbol * denotes a complex conjugate. Figure 8(a) shows the bicoherence $b^2(f=300\ \text{Hz}, f_1)$ with $f=f_1+f_2=300$ Hz (which corresponds to the slow variation in the shear flow). This result shows that the slowly varying shear flow (denoted here as a ZF) is nonlinearly coupled to other frequencies, which can be identified by examining $b^2(f,f_1)$ shown in Fig. 8(b). It is clear that the low frequency ZF is coupled with fluctuations with frequencies in the range of ~5 up to ~11 kHz, which is DWT frequency; the coupling with fluctuations near 8–10 kHz appears to be particularly strong. A detailed measure of the nonlinear energy transfer between the different frequency ranges using cross-bispectral analysis with a two-field model of the fluctuations has shown that the kinetic energy is indeed transferred from these 8–10kHz DWT to large-scale slow evolving shear flow.[18]

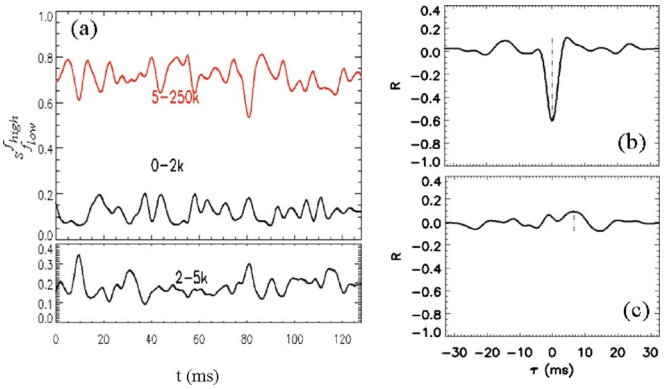

FIG. 9. (Color online) (a) Time-varying DWT kinetic energy in different frequency ranges, 5–250 kHz, 2–5 kHz, and 0–2 kHz. (b) Cross-correlation between high frequency kinetic energy (5–250 kHz) and low frequency kinetic energy (0–2 kHz). (c) Cross-correlation between intermediate frequency range (2–5 kHz) and low frequency range (0–2 kHz) kinetic energy.

Additional evidence showing a link between the time-varying ZF and the DWT comes from examining the relationship between the turbulence kinetic energy and the ZF energy in the time domain. However, this comparison is complicated by the results above which show that the density gradient is modulated. Since this gradient is the principle drive behind the DWT, the resulting energy contained in the DWT can vary due simply to this change in linear drive since the estimated growth rates are sufficiently fast for the DWT amplitude to increase during one oscillation of the ZF. To account for this effect, we examine the variation in the fluctuating ZF and DWT energy normalized to the total fluctuating energy[19] to study the exchange of energy between the DWT and ZF range of frequencies. Here, the normalized power is defined as $s^{f_{\text{high}}}_{f_{\text{low}}}=\int_{f_{\text{low}}}^{f_{\text{high}}}P(f)df/\int_0^{\infty}P(f)df$. Where $P(f)$ is the sum of the radial and azimuthal electric field spectrum. The ZF frequency range is taken to be 0–2 kHz, while the DWT frequency range is taken to be 5 kHz to Nyquist frequency 250 kHz. Figure 9(a) shows the normalized powers fractions $s^{f_{\text{high}}}_{f_{\text{low}}}$ of three different frequency ranges (5–250 kHz, 2–5 kHz, and 0–2 kHz) corresponding to the DWT, intermediate frequency (IF), and ZF frequency ranges. Figures 9(b) and 9(c) show the cross-correlation between high frequency range (5–250 kHz) and ZF frequency range
(0–2 kHz) and between the IF range (2–5 kHz) and ZF range (0–2 kHz), respectively. It is found there is a strong anticorrelation between the high frequency turbulence and the low frequency range, while there is no significant correlation between the intermediate frequency range and the low frequency range. This suggests a direct energy exchange between fluctuations of high frequency and low frequency ranges, consistent with an exchange of energy between the DWT kinetic energy and ZF energy. Similar results are also reported in the literature.[19] We note that by doing normalization, we force the total energy to be constant 1, and this may overemphasize the correlation between the high frequency and low frequency ranges. We have repeated this analysis without this normalization (and thereby ignoring the effect of

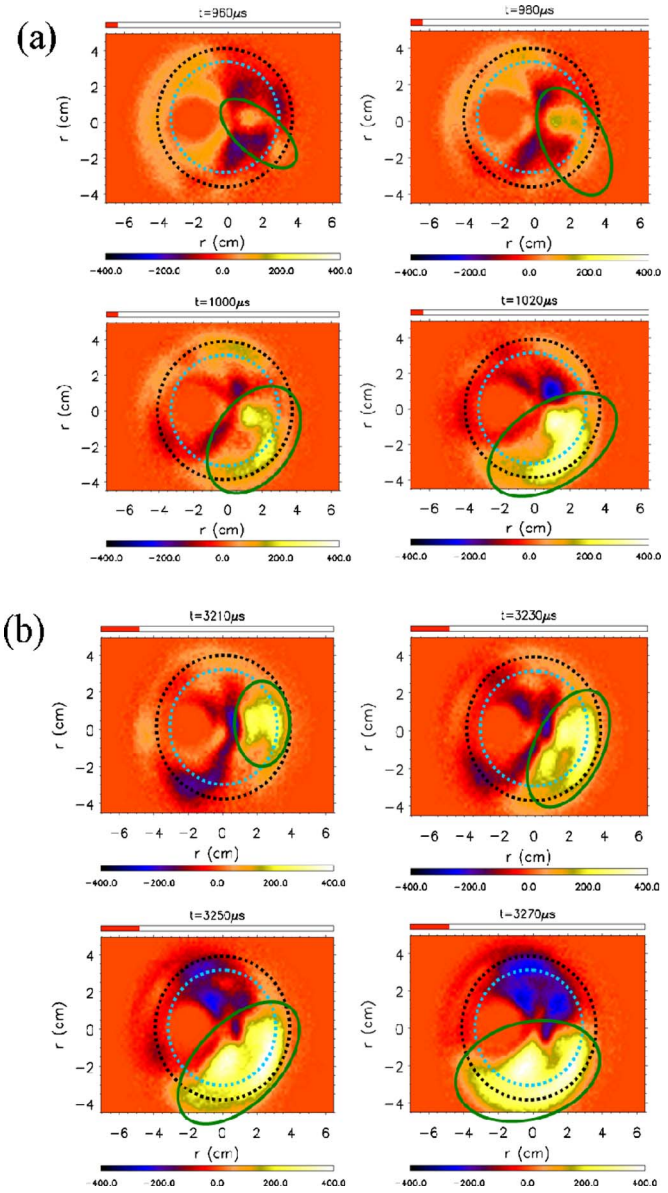

FIG. 10. (Color online) (a) Snapshots of the four consecutive density fluctuation images with 20 μs time interval for strong shear case. (b) Snapshots of the four consecutive density fluctuation images with 20 μs time interval for weak shear case. The outer dashed line indicates the peak shear location, the inner dashed line indicates the maximal density gradient location, and the solid ellipse indicates the positive visible light perturbation structure.

the change in mean gradient) and find a cross-correlation of -0.3 peaking at zero-time-delay for the ZF-DWT case, consistent with an antiphased relationship between these two spectral components.

IV. EFFECT OF SHEAR FLOW BACK ON THE TURBULENCE FROM FAST-FRAMING IMAGING

The effect of the ZF on the radial and azimuthal scale lengths of the DWT is also of interest. This process can be visualized by selecting a sequence of fast-framing images obtained in both the strong shear case and the weak shear case. A representative example is shown in Figs. 10(a) and 10(b), which provide two sets of four consecutive images of the density fluctuation with time interval of 20 μs for strong shear case [the case shown in Fig. 2(a) by the red line, which is around 830 μs] and weak shear case [the case shown in Fig. 2(a) by the yellowish line, which is around 2820 μs], respectively (color bar is an arbitrary unit). It is found that for the strong shear case [Fig. 10(a)], the positive visible light perturbation, which is highlighted by a green ellipse, is formed near the density gradient maximum (indicated by the dashed blue circle) and moves outward radially and azimuthally in the clockwise direction. As it approaches the shear layer (indicated by the dashed black circle), the structure is distorted in the azimuthal direction and eventually becomes highly elongated azimuthally. During this process the radial scale length of the structure is reduced from ~ 2 cm to less than ~ 1 cm. In contrast, during periods of weak flow shear [Fig. 10(b)], the positive visible light perturbation is not distorted during the radial and azimuthal propagations, as a result there is no observable reduction in the radial scale length. This phenomenon suggests a time-varying shear decorrelation process of turbulence structure by the shear flow. For the typical conditions of our experiment, we find the turbulence correlation time τ_c is ~ 50 μs, so the turbulence decorrelation rate, $\omega_T = 1/\tau_c$, is $\sim 2\times 10^4$ 1/s. In the strong shear case the shearing rate defined as $\omega_s = r(d/dr)(v_\theta/r)$ at $r\sim 3.6$ cm is estimated to be $\sim 4\times 10^4$ 1/s, while for the weak shear case, the shearing rate is estimated to be $\sim 0.7\times 10^4$ 1/s. Therefore in the strong shear case, the shear flow is sufficient to have impact on the turbulence,[20] while for the weak shear case it is not, and that when the shear is strong (weak), the radial scale length of the turbulent structure is small (large).

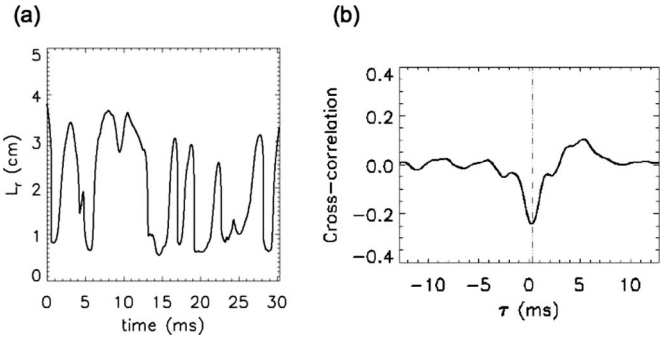

FIG. 11. (a) Time trace of radial correlation length. (b) Cross-correlation between the azimuthal velocity shear and the radial turbulence correlation length at shear location $r\sim 3.6$ cm.

We can also statistically test this picture by using the imaging data to compute the time-varying radial correlation length from a long series of images obtained at ~ 100 kHz framing rate over a period of 240 ms. The radial turbulence correlation length at any point in time is obtained by computing the cross-correlation (using ~ 1 ms time window) between the fluctuating intensity as a function of the radial separation between a reference point located at $r=3.6$ cm and a second point located at a variable radial separation. The cross-correlation function envelope is then used to find the correlation length, defined as the location where the en-

velope is down by a factor of $1/e$ from the peak value at zero spatial separation. This correlation length then varies in time, and this variation can then be cross-correlated with the time variation of the shearing rate. Figure 11(a) is an example of the time trace of the radial correlation length, and Fig. 11(b) shows the correlation between radial correlation length and flow shear at $r \sim 3.6$ cm, which is the shear layer location. We find that there is a finite anticorrelation, confirming that the radial turbulent correlation length is related to the shearing rate, qualitatively consistent with the theoretical picture of the shearing effect of the ZF on the turbulence.[3]

V. DISCUSSION

The above results demonstrate all of the essential elements of the theoretically predicted ZF-DWT dynamics. An existence of the slowly varying azimuthally symmetric ZF has been demonstrated from both probe-based measurements and fast-framing imaging. Such slowly varying ZF is found to modulate the high frequency floating potential associated with DWT, density gradient, and cross-field transport. A strong anticorrelation is found between normalized DWT kinetic energy (5–250 kHz) and the ZF energy (0–2 kHz) but not between the intermediate frequency range (2–5 kHz) and ZF. This suggests a direct energy exchange between DWT and ZF. Comparing with the theory of the modulation instability in which the small seeded shear flow will scatter energy from turbulence to shear flow resulting in amplification of the shear flow and the total energy is conserved, the results shown here is qualitatively consistent with this picture. The momentum balance analysis has shown that such energy exchange is also mediated by the turbulent Reynolds stress or, equivalently, by the bicoherence or the three-wave coupling of the DWT and ZF. Fast-framing imaging has shown an existence of the strong and weak shear flow and found that when the shear flow is strong, the radial correlation length is small, and vice versa. These results suggest that the ZF can shear apart and decorrelate the DWT structures that move into the ZF, which is also qualitatively consistent with the theory predicted decorrelation process of turbulence.

It is also interesting to note that the imaging data show a dominant $m=1$ pattern when the shearing is weak, while the fluctuations have smaller spatial scales in periods with stronger flow shear. In previous work[15,21] such $m=1$ flow patterns have been found to be associated with the formation of blobs or intermittent edge transport events in which a burst of dense plasma breaks off from the central plasma region and propagates outward into the low density halo region surrounding the main plasma column. The results reported here suggest that the shear flow dynamics may be linked to the birth of such intermittent transport events. A detailed study is needed to determine if indeed this is the case.

VI. SUMMARY

In summary we have presented experimental results that are qualitatively consistent with the theoretic picture of the DWT/ZF dynamics. The slowly evolving ZFs are found to exist and do modulate plasma turbulence and resultant transport. ZFs can shear turbulent eddies and reduce the radial correlation length. Energy is exchanged between DWT and ZF and is mediated by the slowly varying turbulent Reynolds stress. Therefore the experimental results support the theoretic expectation of the DWT-ZF dynamics. Future work will be focused on studying the nonlinear energy transfer from DWT to the ZF by bispectral analysis from two-field model in the frequency domain, which will be an additional important evidence of the ZF generation from DWT.

ACKNOWLEDGMENTS

The authors wish to thank P. H. Diamond for many valuable suggestions and conversations. This research was performed under the U.S. Department of Energy (DOE) under Grant No. DE-FG02-06ER54871.

[1] S. I. Braginskii, Rev. Plasma Phys. **1**, 205 (1965).
[2] X. Garbet, Plasma Phys. Controlled Fusion **43**, A251 (2001).
[3] P. H. Diamond, Plasma Phys. Controlled Fusion **47**, R35 (2005).
[4] K. Itoh, S.-I. Itoh, P. H. Diamond, T. S. Hahm, A. Fujisawa, G. R. Tynan, M. Yagi, and Y. Nagashima, Phys. Plasmas **13**, 055502 (2006).
[5] A. Fujisawa, T. Ido, A. Shimizu, S. Okamura, K. Matsuoka, H. Iguchi, Y. Hamada, H. Nakano, S. Ohshima, K. Itoh, K. Hoshino, K. Shinohara, Y. Miura, Y. Nagashima, S.-I. Itoh, M. Shats, H. Xia, J. Q. Dong, L. W. Yan, K. J. Zhao, G. D. Conway, U. Stroth, A. V. Melnikov, L. G. Eliseev, S. E. Lysenko, S. V. Perfilov, C. Hidalgo, G. R. Tynan, C. Holland, P. H. Diamond, G. R. McKee, R. J. Fonck, D. K. Gupta, and P. M. Schoch, Nucl. Fusion **47**, S718 (2007).
[6] K. C. Shaing and E. C. Crume, Jr., Phys. Rev. Lett. **63**, 2369 (1989).
[7] G. R. Tynan, R. A. Moyer, M. J. Burin, and C. Holland, Phys. Plasmas **8**, 2691 (2001).
[8] C. Holland, J. H. Yu, A. James, D. Nishijima, M. Shimada, N. Taheri, and G. R. Tynan, Phys. Rev. Lett. **96**, 195002 (2006).
[9] P. H. Diamond, M. N. Rosenbluth, E. Sanchez, C. Hidalgo, B. Van Milligen, T. Estrada, B. Brañas, M. Hirsch, H. J. Hartfuss, and B. A. Carreras, Phys. Rev. Lett. **84**, 4842 (2000).
[10] P. H. Diamond and Y.-B. Kim, Phys. Fluids B **3**, 1626 (1991).
[11] G. R. Tynan, A. D. Bailey III, G. A. Campbell, R. Charaton, A. de Chambrier, G. Gibson, D. J. Hemker, K. Jones, A. Kuthi, C. Lee, T. Shoji, and M. Wilcoxson, J. Vac. Sci. Technol A **15**, 2885 (1997).
[12] M. J. Burin, G. R. Tynan, G. Y. Antar, N. A. Crocker, and C. Holland, Phys. Plasmas **12**, 052320 (2005).
[13] Z. Yan, J. H. Yu, C. Holland, M. Xu, S. H. Muller, and G. R. Tynan, Phys. Plasmas **15**, 092309 (2008).
[14] G. R. Tynan, C. Holland, J. H. Yu, A. James, D. Nishijima, M. Shimada, and N. Taheri, Plasma Phys. Controlled Fusion **48**, S51 (2006).
[15] G. Y. Antar, J. H. Yu, and G. Tynan, Phys. Plasmas **14**, 022301 (2007).
[16] J. H. Yu, C. Holland, G. R. Tynan, G. Antar, and Z. Yan, J. Nucl. Mater. **363–365**, 728 (2007).
[17] E. J. Powers, J. Y. Hong, and C. P. Ritz, Applied Digital Time Series Analysis (Preliminary Version), University of Texas at Austin (1986).
[18] M. Xu, G. R. Tynan, C. Holland, Z. Yan, S. H. Muller, and J. H. Yu, Phys. Plasmas **16**, 042312 (2009).
[19] A. Fujisawa, A. Shimizu, H. Nakana, S. Ohsima, K. Itoh, H. Iguchi, K. Matsuoka, S. Okamura, S.-I. Itoh, and P. H. Diamond, Plasma Phys. Controlled Fusion **48**, A365 (2006).
[20] H. Biglari, P. H. Diamond, and P. W. Terry, Phys. Fluids B **2**, 1 (1990).
[21] T. Windisch, O. Grulke, and T. Klinger, Phys. Plasmas **13**, 122303 (2006).